ELSEVIER

Journal of Nuclear Materials 244 (1997) 177–184

journal of nuclear materials

Radiation effects in materials for accelerator-driven neutron technologies

M.S. Wechsler [a,*], C. Lin [a], W.F. Sommer [b], L.L. Daemen [b], P.D. Ferguson [b]

[a] North Carolina State University, Raleigh, NC 27695, USA
[b] Los Alamos National Laboratory, Los Alamos, NM 87545, USA

Received 30 May 1996; accepted 7 October 1996

Abstract

Accelerator-driven neutron technologies include facilities for neutron scattering research, accelerator transmutation of waste (ATW), and accelerator production of tritium. These systems use spallation neutron sources (SNS's) in which high-energy protons ($E = 1000$–2000 MeV) strike a heavy-metal target, producing spallation neutrons with energies extending up to the incident proton energy. The nature of the spallation process and the codes used to calculate spallation radiation damage are reviewed. Calculations of displacement and helium production in a major target material, tungsten, are described. Displacement cross sections reach about 9000 b for 1600 MeV neutrons or protons. In a simulated high-current-density ATW SNS, displacement production rates are about 0.1 and 1 dpa/d due to the spallation neutrons and incident 1600 MeV protons, respectively, and the He production rates are about 1 and 250 appm He/d, respectively. These damage rates probably represent an upper limit to what can be tolerated. More realistic solid-target SNS's will operate at lower current densities, and the damage rates are likely to be reduced by a factor of 3 or 4 from the values cited above. In any case, however, radiation damage to target and container materials is a major consideration in the design of SNS's.

1. Introduction

Accelerator-driven neutron technologies use spallation neutron sources (SNS's) in which high-energy protons bombard a heavy-element target and spallation neutrons are produced. For spallation to occur, the energy of the proton must be sufficiently high so that its DeBroglie wavelength is short compared to the size of the target nucleus, thus enabling the incident proton to interact separately with individual nucleons within the nucleus. The DeBroglie wavelength is given by

$$\lambda = h/p \tag{1}$$

where h is Planck's constant and p is the momentum of the proton, given by

$$p^2 = E(E + 2E_0)/c^2 \tag{2}$$

where E is the proton's kinetic energy, E_0 is its rest energy, and c is the speed of light. Thus,

$$\lambda = ch\left[E(E + 2E_0)\right]^{-1/2} \tag{3}$$

For the nuclear radius, we may take as a crude approximation [1]:

$$R = R_0 A^{1/3} \tag{4}$$

where A is the atomic weight of the target nucleus. As pointed out in [1], the nuclear radius does not have a definite value for a given target element, and different types of experiments yield different measures of R (e.g., nuclear-force radius and nuclear-charge radius). Taking the approximate minimum energy for spallation, E_L, as the energy corresponding to the condition $\lambda = R$, we find from Eqs. (3) and (4) that

$$E_L = \left[E_0^2 + (hc/R_0)^2 A^{-2/3}\right]^{1/2} - E_0 \tag{5}$$

Fig. 1 shows E_L versus A, for two values of R_0, 1.1 and 1.6 fm (1 fm = 10^{-15} m) that may be considered to span a

* Corresponding author. 106 Hunter Hill Place, Chapel Hill, NC 27514-9128, USA. Tel.: +1-919 929 5193; fax: +1-919 933 6727; e-mail: wechsler@ncsu.edu.

PII S0022-3115(96)00735-0

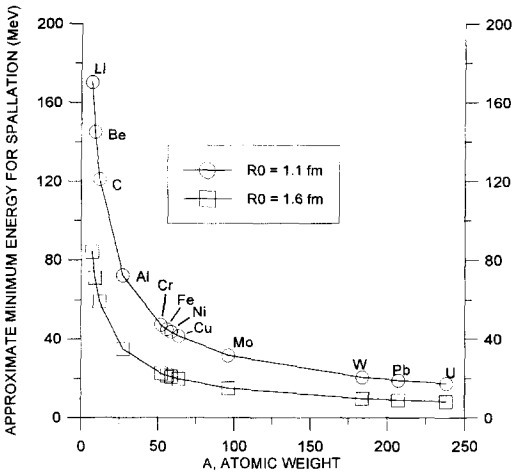

Fig. 1. E_L versus atomic weight of target for two values of R_0 in Eq. (4). E_L is a rough measure of the minimum neutron (or proton) energy for spallation.

reasonable range of possible values [1]. We see that even for the heaviest targets the approximate minimum energy for spallation is likely to be above about 20 MeV and for the lightest targets like Li or Be this energy is much higher. However, Fig. 1 should probably be regarded as being rather conservative; in fact, spallation is generally not considered to be a prominent reaction in the heavy targets unless the proton energies are above about 100 MeV [1,2].

It may have been about 1947 that the term 'spallation' began to be used in the context of nuclear interactions [3,4]. Serber [4] proposed a model in which spallation reactions are considered to occur in two stages, an intranuclear cascade stage followed by a de-excitation stage. In the intranuclear cascade, the incoming projectile collides with one nucleon at a time within the nucleus, and the struck nucleons leave the nucleus with considerable energy. The nucleus, left in an excited state, then de-excites by nucleon evaporation or by fission. In nucleon evaporation, nucleons are ejected until the excitation energy falls below the nucleon binding energy of several MeV, whereupon the remaining energy is removed by gamma-ray emission. As concerns de-excitation by fission, it is perhaps useful to refer to this as high-energy fission, in order to distinguish it from the low-energy fission ($E < \sim 20$ MeV) that occurs in thermal and fast reactors. Low-energy fission shows the familiar double-humped mass yield curve, whereas high-energy fission resulting from spallation gives a broader curve. The spallation product generation rate versus atomic number, Z, of the yielded product is illustrated in Fig. 2, taken from Russell et al. [5] for Pb and W targets bombarded by 1000 MeV protons. We see in Fig. 2 a large product yield near Z of the original target plus a lower single broad peak near $Z/2$. Semi-empirical formulae for cross sections expressing the product yield as a function of Z and A have been given by Rudstam [6] and by Silberberg and Tsao [7,8]. Cloth et al. [9] have noted that the probability that fission occurs during de-excitation is proportional to Z^2/A. Since Z/A is roughly constant over the periodic table (at a value of about 0.45, except for hydrogen), this probability should be approximately proportional to Z.

Spallation-induced high-energy fission may be contrasted to nuclear-reactor low-energy fission in a number of other ways, as is pointed out in [5,10]. The number of neutrons produced by spallation in a heavy target nucleus is quite high; for example, calculations described below indicate that 32 neutrons per proton are produced upon bombardment of tungsten by 1000 MeV protons. By contrast, only about 2.5 neutrons are produced upon low-energy fission of a fissile or fissionable nucleus. Also, the energy distribution of the neutrons is quite different for the two cases. Spallation neutrons have an energy distribution that may be described as a degraded fission spectrum with a high-energy tail that extends up to the incident energy above $\sim$ 100 MeV of the bombarding protons, whereas the average neutron energy in the low-energy fission flux is only 1–2 MeV. Calculated spallation neutron spectra are presented in [11] for 800 MeV protons on Cu and W, and a study of neutron and proton dosimetry at the LAMPF 800 MeV proton accelerator is described in [12]. Furthermore, despite the greater number of neutrons produced in spallation, the energy deposited per neutron produced is less for spallation reactions ($\sim$ 25 MeV) than for low-energy fissions ($\sim$ 180 MeV) [5].

In the above discussion, we have considered the incident projectiles to be protons, but spallation also occurs when the bombarding particles are neutrons (or deuterons, pions, muons, etc.), provided that the condition $\lambda < R$ is satisfied. This means that many of the particles ejected from the nucleus in the initial intranuclear cascade will

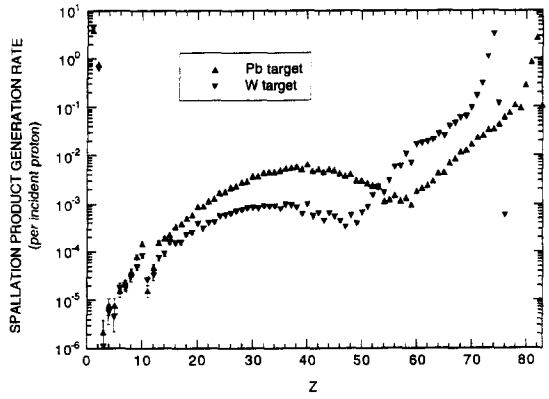

Fig. 2. Spallation product generation rate (number of product nuclei per incident proton) versus atomic number, Z, of the product for Pb and W targets; diameter 0.5 m, length 2 m, bombarded on axis by 1000 MeV protons. After Russell et al. [5].

Table 1
Operating pulsed spallation neutron sources for neutron scattering research

Facility	Site [a]	Beam power (kW)	Beam current (mA)	Proton energy (MeV)	Target
ISIS	RAL, UK	160	0.2	800	U
LANSCE	LANL, USA	48	0.06	800	W
IPNS	ANL, USA	6.8	0.015	450	U
KENS	KEK, Japan	3	0.006	500	U

[a] RAL, Rutherford Appleton Laboratory; LANL, Los Alamos National Laboratory; ANL, Argonne National Laboratory; KEK, National Laboratory for High Energy Physics.

strike other nuclei and produce additional intranuclear cascades there, and the ejected particles may in turn stimulate further spallation events. This succession of events is known as an internuclear cascade. Radiation damage specialists will be aware of the analogy to displacement cascades.

Accelerator-driven spallation neutron sources (SNS's) are found to be extremely useful in facilities for neutron scattering (and diffraction) research. In this application, the incident protons are pulsed at frequencies in the range 10–60 Hz. Presently, there are four operating pulsed SNS's: ISIS, LANSCE, IPNS, and KENS. As noted in Table 1, the highest operating beam power is only 160 kW. There are, however, a number of higher-powered SNS's in various stages of development, ranging from slightly under 1 MW for SINQ (under construction in Switzerland, 1.5 mA beam current, 590 MeV proton energy) to 5 MW for ESS (under design in the European Union, 1330 MeV proton energy) [13]. In addition, studies are underway for higher-powered SNS's for the production of tritium [14] and the transmutation of nuclear waste [15,16]. These are to be continuous-wave systems with beam powers that range up to 200 MW (200 mA beam current, 1000 MeV proton energy), specifications that are believed to be achievable with the present advanced state of accelerator technology [17].

The materials exposed to the most damaging radiation environments in an SNS are those in the path of the incident proton beam. This includes target and window materials. These materials will experience damage from the incident protons and the spallation neutrons. In addition, some materials will be damaged by the spallation neutrons alone. The principal materials of interest for SNS's are discussed in [18,19]. The target should consist of one or more heavy elements, so as to increase the number of neutrons produced per incident proton. A liquid metal target (e.g., Pb, Bi, Pb–Bi, Pb–Mg, and Hg) has the advantage of eliminating the effects of radiation damage on the target material itself, but concerns over corrosion problems and the influence of transmutants remain. The major solid targets in operating SNS's (Table 1) and under consideration for the 1–5 MW SNS's are W, U, and Pb. Tungsten is the target material at LANSCE (Table 1), and is the projected target material for an upgraded LANSCE target that is presently being designed. It is also the projected target material for the tritium-producing SNS under design at LANL [14].

In this paper, we present the results of spallation radiation damage calculations (displacement and He production) for tungsten. Earlier spallation radiation damage results were given for copper [20,21], Inconel 718 [22], stainless steel [23], and tungsten [24].

2. Computer codes

The computer codes used in this investigation are LAHET, MCNP, and SPECTER. LAHET [25] is the LANL version of the High Energy Transport Code, HETC, which was originally developed at ORNL [26]. It calculates the energy and direction of particles ejected from the intranuclear cascades and subsequent evaporation and fission. It also calculates the masses and recoil energies of recoiling nuclei and fission products. An option is available that gives the primary knocked-on atom (PKA) spectrum in terms of the raw recoil energies and the damage energies calculated according to the Lindhard model [27]. This option also gives the average damage energy per incident particle, $\langle T_{\mathrm{dam}} \rangle / n'$, where the average is taken over the n' histories being run. The thin-target damage-energy cross section is then given by

$$\sigma_E = \frac{\langle T_{\mathrm{dam}} \rangle / n'}{N_{\mathrm{V}} x} \tag{6}$$

where N_{V} is the atom density of the target and x is the target thickness. In accord with [28], the displacement cross section is then given by

$$\sigma_{\mathrm{d}} = (\beta / 2T_{\mathrm{d}}) \sigma_E \tag{7}$$

where $\beta = 0.8$ and T_{d} is the (effective) threshold displacement energy. The output for He gas production from LAHET gives the number of helium atoms produced per incident particle, $n(\mathrm{He})/n'$. In analogy to Eq. (6), the helium production cross section is given by

$$\sigma(\mathrm{He}) = \frac{n(\mathrm{He})/n'}{N_{\mathrm{V}} x} \tag{8}$$

For all the LAHET calculations in the present work, the target was assumed to be a circular cylinder, 0.5 m in

radius, with thickness $x = 0.01$ m. The atom density for W was taken to be $N_V = 6.30 \times 10^{28}$ atoms/m^3.

MCNP, the Monte Carlo code for the transport of neutrons and photons [29], is a continuous-energy code that transports neutrons and photons. It contains a sophisticated generalized-geometry utility that permits complex geometries to be modelled, and it employs the ENDF/B cross section library [30]. We use MCNP to evaluate neutron fluxes and spectra.

For assessing radiation damage due to incident neutrons of energies below 20 MeV, we employed the SPECTER code [31], which uses the DISCS program [32] for displacement calculations. The underlying cross sections stem from the ENDF/B libraries [30], and they extend up to 20 MeV. The calculations embrace elastic and inelastic scattering, including thermal neutron capture (n, γ) events. As is the case for LAHET, SPECTER partitions recoil energies into nuclear and electronic components in accord with the Lindhard model [27].

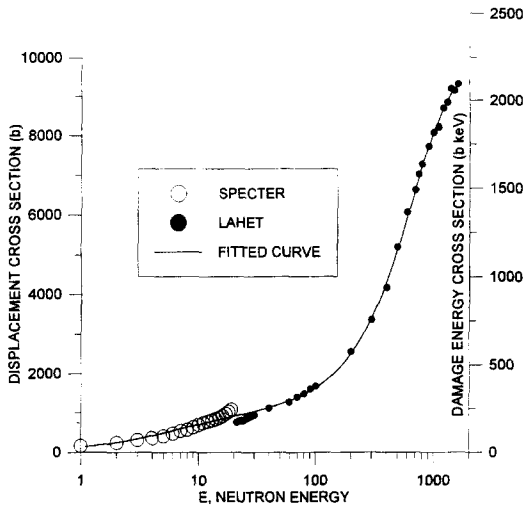

Fig. 4. Damage energy cross section and displacement cross section (using threshold displacement energy 90 eV) versus neutron energy for W as calculated by SPECTER ($E < 20$ MeV) and LAHET ($E > 20$ MeV). A polynomial fitted curve is also shown.

3. Displacement production

Fig. 3 shows the damage-energy cross section and the displacement cross section for tungsten as a function of the energy of incident neutrons or protons from near 20 to 1600 MeV as calculated by LAHET, where the conversion from σ_E in Eq. (6) to σ_d in Eq. (7) involved the use of threshold displacement energy $T_d = 90$ eV [28]. The number of incident neutrons or protons run was 150,000; thus, $\langle T_{dam} \rangle$ in Eq. (6) represents an average over 150,000 histories. We see that the proton cross sections lie distinctly below those for neutrons at energies of about 100 MeV and below, and only slightly below the neutron values at 200 MeV and above. Fig. 4 shows the damage energy and displacement cross sections versus neutron energy for tungsten, where the calculations for $E < 20$ MeV were done by SPECTER and for $E > 20$ MeV by LAHET. The SPECTER output gives displacement cross sections directly for the stable tungsten isotopes, W-182, W-183, W-184, and W-186, which have abundances of 26.3, 14.3, 30.7, and 28.6%. To obtain the plotted values for natural tungsten, we calculated an average weighted over these atomic fractions. The threshold displacement energy used for W in SPECTER was again 90 eV. One sees in Fig. 4 that the LAHET cross section lies somewhat below the SPECTER one at the dividing line energy of 20 MeV between the two sets of calculations. We have observed this to be the case for a number of target materials, as is discussed further below.

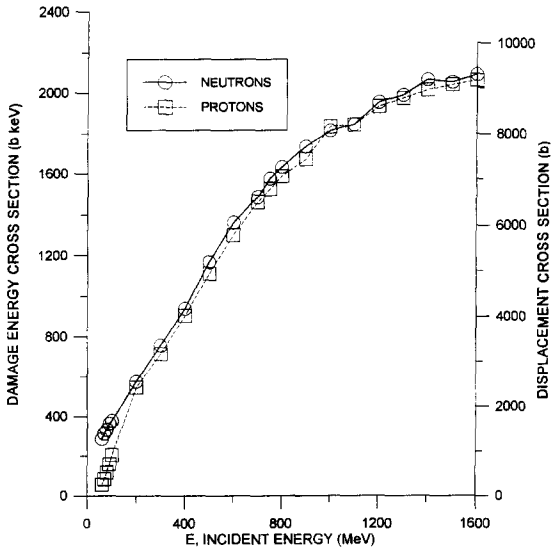

Fig. 3. Damage energy and displacement cross sections for tungsten versus energy of incident particles. Threshold displacement energy 90 eV. LAHET calculations for 150,000 incident neutrons or protons.

The differential displacement production rate is given by

$$K'_d = \sigma_d \phi'_E \tag{9}$$

where ϕ'_E is the differential neutron flux. The exact form of ϕ'_E for an SNS depends, of course, on the particular design of the facility. As an example, we shall use the ϕ'_E that was calculated for an accelerator transmutation of waste (ATW) target consisting of a homogeneous mixture of tungsten and water (0.25 m radius; 85% volume fraction occupied by the tungsten) surrounded by heavy water [22]. The incident protons were assumed to have an energy of 1600 MeV, a current density of about 200 μA/cm^2, and a flat-profile beam radius of 0.2 m. A current density of 200

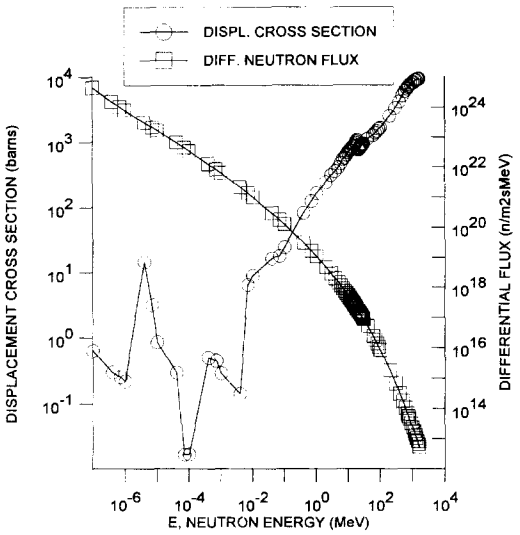

Fig. 5. Displacement cross section for tungsten and differential neutron flux at 0.25 m from the axis of the 1600 MeV proton beam for a simulated ATW SNS [18]. Flux of neutrons of all energies from 0.025 eV to 1600 MeV, 1.3×10^{20} n/m^{2}s.

μA/cm^2 may represent an upper limit, and a more realistic value may well be perhaps one-third of this value. However, 200 μA/cm^2 is being used as a reference parameter for the ESS [13], for which a liquid mercury target is anticipated. At the edge of our target (i.e., at $r = 0.25$ m), the flux of neutrons of all energies down to 0.025 eV was calculated to be 1.3×10^{20} n/m^{2}s. The calculated differential neutron flux and the displacement cross section discussed above are shown in Fig. 5. The somewhat irregular cross section points for energies below about 0.01 MeV are due to (n, γ) recoil events. As

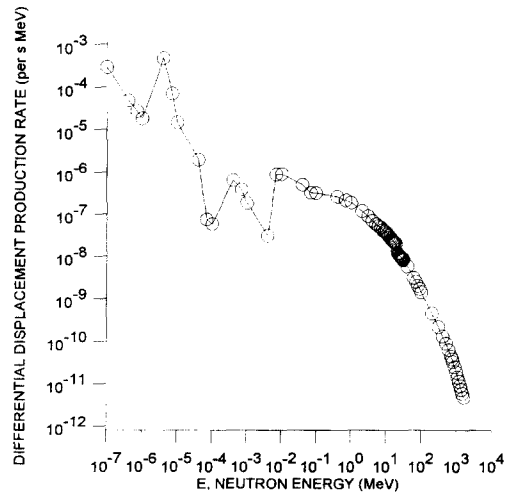

Fig. 6. Differential displacement production rate, K'_d, versus neutron energy for tungsten in the ATW differential neutron flux shown in Fig. 5.

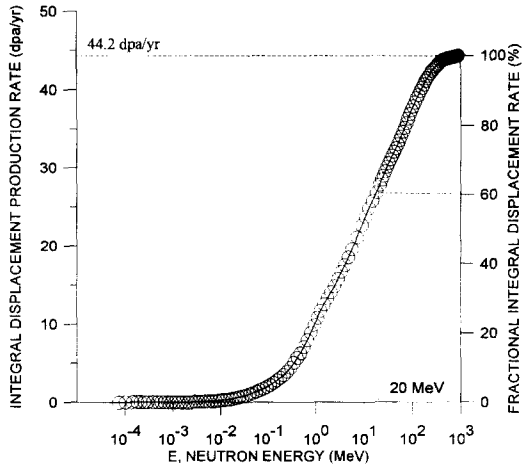

Fig. 7. Integral displacement rate (dpa/s due to neutrons of energies < E) and fractional integral displacement rate (fractional number of dpa's due to neutrons of energies < E) versus neutron energy E.

expected because of the presence of light and heavy water, Fig. 5 indicates a highly moderated neutron spectrum and a large increase in ϕ'_E with decreasing neutron energy, E. The plot in Fig. 6 shows the trend toward increasing K'_d with decreasing E. Nevertheless, as seen in Fig. 7, the displacement production rate due to neutrons in the flux with energies below E begins to rise significantly only for energies above about 0.1 MeV, reaching a displacement rate of 44 dpa/y or 0.12 dpa/d (dpa/day) for neutrons of all energies in the spectrum. Fig. 7 suggests that about 60% of the displacements are due to neutrons with energies below 20 MeV, and the median energy corresponding to fractional integral displacement rate of 0.5 is about 10 MeV.

The displacement production rate for tungsten in the direct proton beam is based on the incident current density

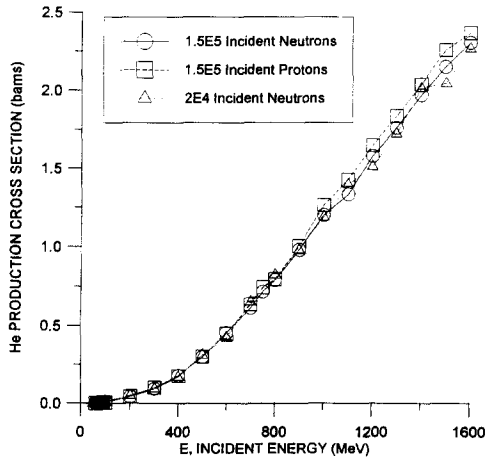

Fig. 8. Helium production cross section versus incident energy for tungsten.

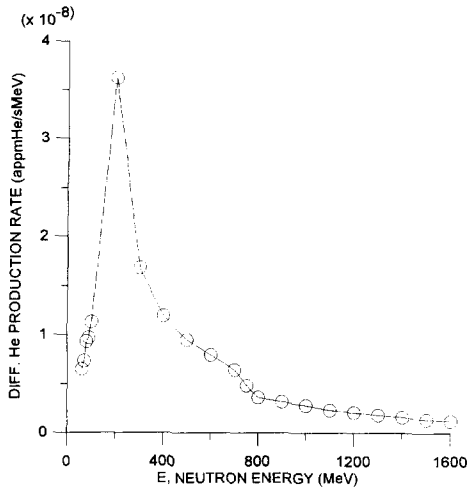

Fig. 9. Differential helium production rate, K'(He), versus neutron energy for tungsten.

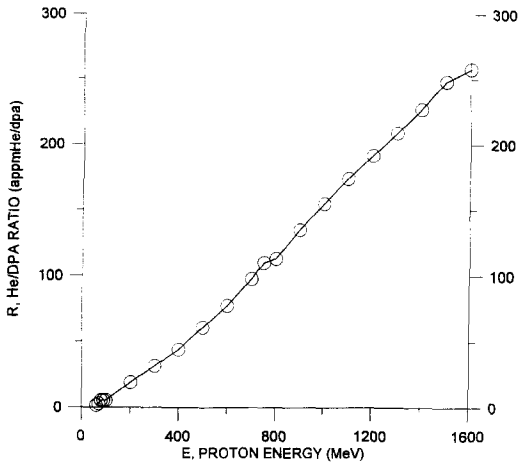

Fig. 11. Helium to dpa ratio, R, versus incident proton energy for tungsten.

of 1600 MeV protons near 200 μA/cm^2 or 1.24×10^{19} p/m^{2}s and the displacement cross section of 9184 b (Fig. 3). This gives $K_d = 0.99$ dpa/d, a quite substantial displacement rate. Bauer et al. [13] cite 2.8 dpa/d for W due to the protons in a 5 MW SNS.

4. Helium production

Fig. 8 gives the He production cross section versus incident energy for 150,000 incident neutrons or protons and 20,000 incident neutrons. The three curves are in reasonable agreement with the He production cross section reaching about 2.5 barns at 1600 MeV. When the neutron cross sections (150,000 histories) are multiplied by the ATW differential flux in accord with the analog to Eq. (9), we find that the differential helium production rate rises to a peak at about 200 MeV (Fig. 9) and then decreases monotonically upon further increase in neutron energy.

Integrating K'(He) in Fig. 9 from 0 to E, we obtain the helium production rate due to neutrons of energies below E (Fig. 10). The production rate for all neutrons up to 1600 MeV is 1.02 appm He/d. Fig. 10 also shows f, the fractional He production rate in the ATW spectrum. The median neutron energy corresponding to $f = 0.5$ is about 330 MeV.

To obtain the helium production rate in W subjected to the direct 1600 MeV proton beam, we use the cross section of 2.37 b (Fig. 8) and again the incident flux of 1.24×10^{19} p/m^{2}s, which gives 254 appm He/d. Bauer et al. [13] estimate 173 appm He/d for W in a 5 MW SNS.

It is often of interest to examine the ratio, R, of the helium and displacement production rates. From the rates given above due to the spallation neutron spectrum, 1.02 appm He/d and 0.12 dpa/d, we get 8.4 appm He/dpa. For the 1600 MeV protons, we calculate 254 appm He/d and 0.99 dpa/d, giving 258 appm He/dpa. The R ratio decreases with decreasing proton energy, as is seen in Fig. 11.

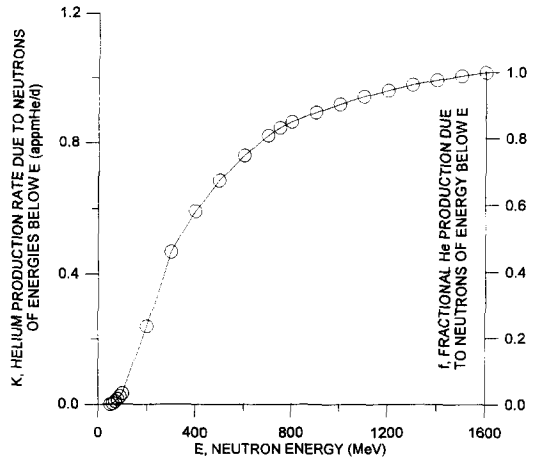

Fig. 10. Integral helium production rate (appm He/s due to neutrons of energies < E) and fractional integral displacement rate (fractional number of He atoms due to neutrons of energies < E) versus neutron energy E for tungsten.

5. Discussion

As mentioned above, the discrepancy at 20 MeV shown in Fig. 4 between displacement cross sections calculated using LAHET and SPECTER has been observed for a number of materials, the LAHET cross section always lying below the SPECTER one. In addition, there seems to be a trend toward greater relative discrepancy for lighter target materials. Fig. 1 shows that the approximate mini-

mum energy for spallation increases with decreasing atomic weight of the target material. This suggests that the condition for spallation is more difficult to achieve in the lighter targets, and therefore the discrepancy may be associated with lack of validity in the intranuclear cascade model at energies as low as 20 MeV. Another possibility is that LAHET does not transport neutrons below 20 MeV, so that the displacement production due to neutrons leaving a reaction with energies below 20 MeV is not taken into account. Fig. 4 shows that the discrepancy for W is not large, but this is a matter that will receive further investigation.

The results of our calculations concerning the displacement production indicate rates of 0.12 and 0.99 dpa/d due to the spallation neutrons and the incident protons, respectively, or a total of about 1.1 dpa/d. A rough indication of the consequences of this radiation exposure may be obtained by considering the effect of fission reactor irradiation on the ductility of tungsten. Krautwasser et al. [33] studied the effect of irradiations at about 250–300°C in the FRJ2 reactor at Jülich and the HFR reactor at Petten on the ductile–brittle properties of pure W and two tungsten alloys as revealed by three-point bending tests. The pure W showed the least effect of the irradiation. But, even for the pure W, exposure to 1.1 dpa produced an increase in the ductile–brittle transition temperature of 485°C. For the full 200 $\mu A/cm^2$ (1.2×10^{19} p/m^2s) proton beam, this suggests that after only one day in the SNS, the W target rods would be operating well into the brittle domain. For a proton beam with one-third of this current density, the time for a 485°C increase in the ductile–brittle transition temperature would still be only three days. This may be a matter of some concern, possibly suggesting that the target rods should be clad in a more radiation resistant envelope, even though the target rods will probably have low loads applied to them.

Green et al. [34] presented the results of HETC calculations of displacement and He production for 600 and 750 MeV protons and measured He production for 750 MeV protons on W and other metals. The calculations were performed using HETC, and the measurements employed mass spectrometry following vacuum vaporization in a resistance-heated graphite crucible. The calculated results of Green et al. for the average damage energy per recoil and the damage energy, displacement, and helium cross sections for 600 and 750 MeV protons on W and their measured He production cross section for 750 MeV protons are shown in Table 2. The results of the present study are also shown for comparison. The calculated $\langle T_{dam} \rangle$ per recoil, σ_E, and σ_d in the present study are somewhat lower than those calculated by Green et al., but nevertheless in reasonable agreement. However, for the He cross section for 750 MeV protons, the value calculated by Green et al. is much greater than the measured value, whereas the value calculated in the present work, 0.74 b, is quite close to the measured cross section, 0.76 b. The

Table 2
Comparison of present work with Green et al. [34]

	Green et al., measured	Green et al., calculated	Present work, calculated
$\langle T_{dam} \rangle$ per recoil (keV)			
600 MeV p's		658	641
750 MeV p's		722	688
σ_E (b keV)			
600 MeV p's		1533	1356
750 MeV p's		1743	1578
σ_d (b)			
600 MeV p's		6813	6065
750 MeV p's		7747	7015
σ(He) (b)			
600 MeV p's			0.452
750 MeV p's	0.762	2.109	0.744
R (appm He/dpa)			
600 MeV p's		245	75
750 MeV p's	98 [a]	272	106

[a] R = appm He (measured)/dpa (calculated).

reason for the discrepancy in the measured and calculated 750 MeV proton cross sections, 0.76 and 2.11 b, respectively, in the Green et al. study is not clear, but one possibility lies in the selected nuclear level density option. In our version of LAHET, this refers to the 13th data item in record 4, ILVDEN. This item has three options as indicated in [25]: option 1, the original HETC level density formulation; option 2, the Gilbert–Cameron–Cook–Ignatyuk level density model (default option), and option 3, the Jülich level density parametrization as a function of mass number. In all of our results presented in this paper, we have used option 2, which gives the He production cross section of 0.74 b for 750 MeV protons on W, as shown in Table 2. But, we have also done the calculation for 750 MeV protons on W using the other two options. Option 1 gives 0.89 b and option 3 gives 2.45 b. Thus, the calculated He production can depend greatly on the ILVDEN option selected. The above discussion indicates the importance of stating the particular options that are used in reporting the results of HETC and LAHET calculations. But chiefly, perhaps, it indicates that the codes need to be checked by comparison with experimental results wherever possible.

6. Summary

SPECTER calculations for neutron and proton energies below 20 MeV and LAHET calculations above 20 MeV were used to calculate displacement cross sections for tungsten. The displacement cross section for tungsten rises to about 9000 b for 1600 MeV neutrons or protons. The

total displacement rate in a neutron spectrum based on a simulated ATW SNS with incident proton current density of 200 $\mu A/cm^2$ is calculated to be about 0.12 dpa/d due to the spallation neutrons, and about 60% of the displacements are due to neutrons below 20 MeV. For tungsten in the direct proton beam, the displacement rate is about 1 dpa/d. The helium production rate in the ATW spectrum of spallation neutrons and in the direct 200 $\mu A/cm^2$ proton beam are calculated to be 1.0 and 254 appm He/d, respectively. The current density of 200 $\mu A/cm^2$ may represent an upper limit to what is achievable, with more reasonable levels reduced from these by a factor of about 1/3. However, even for this lower-current-density case, radiation damage to the tungsten target rods is likely to be substantial.

References

[1] G. Friedlander, J.W. Kennedy, E.S. Macias and J.M. Miller, Nuclear and Radiochemistry (John Wiley and Sons, New York, 1981).

[2] I. Kaplan, Nuclear Physics (Addison-Wesley Publishing Company, Reading, MA, 1962).

[3] G.T. Seaborg, Chem. Eng. News 25 (1947) 2819.

[4] R. Serber, Phys. Rev. 72 (1947) 1114.

[5] G.J. Russell, E.J. Pitcher and L.L. Daemen, in: AIP Conf. Proc. 346 (American Institute of Physics, Woodbury, NY, 1995) p. 93.

[6] G. Rudstam, Z. Naturforsch. 21a (1966) 1027.

[7] R. Silberberg and C.H. Tsao, Astrophys. J. Suppl. 25 (1973) 315.

[8] R. Silberberg and C.H. Tsao, Astrophys. J. Suppl. 25 (1973) 335.

[9] P. Cloth, D. Filges and R. Hecker, Atom-Kernenergie 41 (1982) 243.

[10] L.L. Daemen, P.D. Ferguson, W.F. Sommer and M.S. Wechsler, in: AIP Conf. Proc. 346 (American Institute of Physics, Woodbury, NY, 1995) p. 488.

[11] W.F. Sommer, P.D. Ferguson and M.S. Wechsler, J. Nucl. Mater. 191–194 (1992) 1374.

[12] D.R. Davidson, Ph.D. thesis, Iowa State University, Ames, IA (1990).

[13] G. Bauer, F. Atchison, T.A. Broome and H.M. Conrad, in: AIP Conf. Proc. 346 (American Institute of Physics, Woodbury, NY, 1995) p. 105.

[14] M. Cappiello, P. Lisowski, G.J. Russell and S.C. Rose, in: AIP Conf. Proc. 346 (American Institute of Physics, Woodbury, NY, 1995) p. 865.

[15] C.D. Bowman, in: AIP Conf. Proc. 346 (American Institute of Physics, Woodbury, NY, 1995) p. 22.

[16] C.D. Bowman, E.D. Arthur, P.W. Lisowski, G.P. Lawrence, R.J. Jensen, J.L. Anderson, B. Blind, M. Cappiello, J.W. Davidson, T.R. England, L.N. Engel, R.C. Haight, H.G. Hughes, J. Ireland, R.A. Krakowski, R.J. LaBauve, B.C. Letellier, R.T. Perry, G.J. Russell, K.P. Staudhammer, G. Versamis and W.B. Wilson, Nucl. Instrum. Methods A 320 (1992) 336.

[17] T.P. Wangler, in: AIP Conf. Proc. 346 (American Institute of Physics, Woodbury, NY, 1995) p. 937.

[18] M.S. Wechsler, J.F. Stubbins, W.F. Sommer, P.D. Ferguson and E.H. Farnum, Selection and Qualification of Materials for the Accelerator Transmutation of Waste Project, Los Alamos National Laboratory Report LA-UR-92-1211, Los Alamos, NM 87545 (1992).

[19] J.F. Stubbins, M.S. Wechsler, M. Borden and W.F. Sommer, in: AIP Conf. Proc. 346 (AIP Press, American Institute of Physics, Woodbury, NY, 1995) pp. 879–888.

[20] M.S. Wechsler and W.F. Sommer, J. Nucl. Mater. 122–123 (1984) 1078.

[21] M.S. Wechsler, D.R. Davidson, L.R. Greenwood and W.F. Sommer, in: Effects of Radiation on Materials, STP 870, eds. F.A. Garner and J.S. Perrin (ASTM, Philadelphia, 1985) p. 1189.

[22] M.S. Wechsler, P.D. Ferguson, C. Lin and W.F. Sommer, in: Reactor Dosimetry, STP 1228, eds. H. Farrar, E.P. Lippincott, J.G. Williams and D.W. Vehar (ASTM, Philadelphia, 1994) p. 782.

[23] M.S. Wechsler, R. Ramavarapu, E.L. Daugherty, R.C. Palmer, D.B. Bullen and W.F. Sommer, J. Nucl. Mater. 212–215 (1994) 1678.

[24] M.S. Wechsler, C. Lin and W.F. Sommer, in: AIP Conf. Proc. 346 (American Institute of Physics, Woodbury, NY, 1995) p. 466.

[25] R.E. Prael and H. Lichtenstein, User Guide to LCS: The LAHET Code System, Los Alamos National Laboratory Report LA-UR 89–3014 (1989).

[26] K.C. Chandler and T.W. Armstrong, Operating Instructions for the High Energy Nucleon–Meson Transport Code, HETC, Oak Ridge National Laboratory Report ORNL-4744 (1972).

[27] J. Lindhard, V. Nielsen, M. Scharff and P.V. Thomsen, K. Dan. Vidensk. Selsk. Mat. Fys. Medd. 33(10) (1963).

[28] Standard Practice for Neutron Radiation Damage Simulation by Charged-Particle Irradiation, E 521-96, Annual Book of ASTM Standards, Vol. 12.02 (American Society for Testing and Materials, Philadelphia, 1996) p. 1.

[29] J.F. Briesmeister, ed., MCNP – A General Monte Carlo Code for Neutron and Photon Transport, Version 3A, Los Alamos National Laboratory Report LA-7396-M, Rev. 2 (1986).

[30] O. Ozer and D. Garber, ENDF/B Summary Documentation, Brookhaven National Laboratory Report BNL-17541 (1973).

[31] L.R. Greenwood and R.K. Smither, SPECTER: Neutron Damage Calculations for Materials Irradiations, Argonne National Laboratory Report ANL/FPP/TM-197 (1985).

[32] G.R. Odette and D.R. Doiron, Nucl. Technol. 29 (1976) 346.

[33] P. Krautwasser, H. Derz and E. Kny, High Temp. High Pressures 22 (1990) 25.

[34] S.L. Green, W.V. Green, F.H. Hegedus, M. Victoria, W.F. Sommer and B.M. Oliver, J. Nucl. Mater. 152–157 (1988) 1350.